JOURNAL OF MATERIALS SCIENCE 12 (1977) 234–238

Diffraction contrast of fold domain boundaries in polyethylene single crystals

EDWIN L. THOMAS
Department of Chemical Engineering and Materials Science, University of Minnesota, Minneapolis, Minnesota, USA

The dark-field diffraction contrast images of several types of fold domain boundaries in polyethylene single crystals have been characterized. Macrosector, microsector, {1 1 0} and {3 1 0} twin boundary contrast are shown to be due to the image shift which occurs when two diffracted beams contribute to the dark-field image.

1. Introduction

Since their discovery, polyethylene single crystals have been envisaged as consisting of folded chain molecules with the plane of chain folding parallel to the growth face. Such an arrangement causes the formation of boundaries along the intersection of the growth faces where the direction and/or plane of chain folding changes ((macrosector) fold domain boundary) [1]. For diamond-shaped polyethylene single crystals these boundaries are between {1 1 0} planes [2]. Polyethylene crystals also frequently are twinned on {1 1 0} and {3 1 0} planes [2–5] leading to further types of (twin) fold domain boundaries.

Dark-field microscopy shows strong diffraction contrast occurs at macrosector and microsector boundaries as well as twin boundaries, and although the boundaries are similar in nature, the contrast mechanism proposed for each is rather dissimilar.

Bassett [6, 7] examined macrosector and microsector boundaries and attributed the boundary contrast to tilt to the molecules in the plane of the boundary due to the interaction of asymmetrical fold protrusions across the boundaries. Wittmann and Kovacs [4] investigated several types of polyethylene twins and observed that depending on the focal setting of the objective lens the two portions of the twin image could overlap or be separated. They attributed the effect to axial astigmatism of the objective lens.

In the present work the contrast behaviour of all three types of fold domain boundary is shown to result from the image shift due to two diffracted beams of different azimuthal angle α and scattering angle β contributing to the dark-field image.

2. Mechanism of image shift

Consider two diffracted beams differing only slightly in their diffraction vector g so that both beams can easily pass through the objective aperture (see Fig. 1a). The image of the specimen will consist of the image of the $(h_1k_1l_1)$ planes and the image of $(h_2k_2l_2)$ planes. Owing to spherical aberration, axial astigmatism and defocusing errors the images of both sets of planes will not come to focus in the same plane [8]. The image shift ΔX_j for each set of planes will be:

$$\Delta X_j = MC_s\beta_j^3 + M\Delta f_{ast}\beta_j \sin\alpha_j + M\Delta f\beta_j$$

where C_s is the spherical aberration coefficient of objective lens, $\Delta f_{ast} = f_{90°} - f_{0°}$ = difference of focus of objective lens due to astigmatism, M is the magnification, Δf is the amount of defocus of the objective lens, α_j the azimuthal angle of beam j, and β_j the scattering angle of beam j. The image shift for each dark-field image will be parallel to the diffraction vector so that the observed image shift direction will be along:

$$\Delta g = g_1 - g_2$$

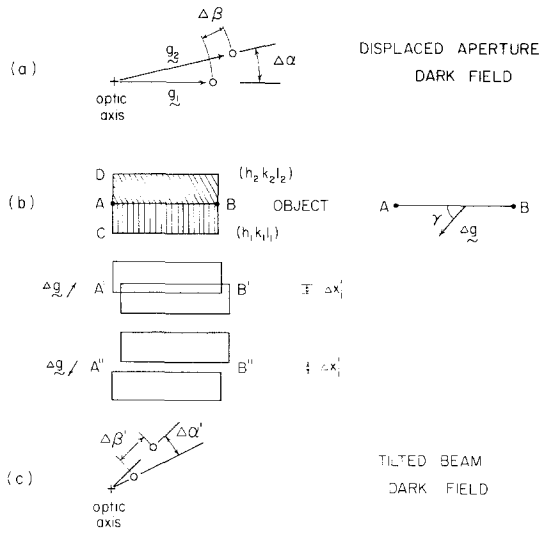

Figure 1 (a) Diffraction condition for two beam displaced aperture dark field. (b) The contrast along the boundary $\overline{AB}$ from a crystal containing two domains each imaged by a separate set of diffracting planes will be either bright, dark or show no contrast, dependent on the image overlap, $\Delta X_i'$. (c) Diffraction condition for two beam tilted beam dark field.

The image overlap $\Delta X_i'$ is therefore:

$$\Delta X_i' = [MC_s(\beta_1^3 - \beta_2^3) + M\Delta f(\beta_1 - \beta_2) + M\Delta f_{ast}(\beta_1 \sin\alpha_1 - \beta_2 \sin\alpha_2)] \sin\gamma$$

where γ is the angle between Δg and the domain boundary (see Fig. 1b).

The contrast from a crystal containing two adjacent domains each imaged by a separate set of diffracting planes will be either bright (positive overlap), dark (negative overlap) or show no contrast (no overlap) depending on $\Delta X_i'$ (see Fig. 1b). The exact value of $\Delta X_i'$ will also depend on whether displaced aperture or tilted beam dark field is employed. For displaced aperture dark field, $\Delta\alpha$ and $\Delta\beta$ can be calculated from the diffraction pattern (see Table I) whereas $\Delta\alpha$ and $\Delta\beta$ become dependent on the precise setting of the diffracted beams relative to the optical axis for tilted beam dark field (see Fig. 1c). For resolutions* of the order of 50 Å, we can neglect the contribution to $\Delta X_i'$ from spherical aberration. For defocusing and astigmatism of the order of 10^5 Å (due to operation at low – 1000 × to 3000 × – magnification) we see that for good boundary visibility (say $\geqslant$ 100 Å boundary width) $\Delta\alpha \geqslant 10^{-1}$ rad and $\Delta\beta \geqslant 10^{-3}$ rad. Boundaries which are parallel to Δg (e.g. g_1, g_2, are approximately normal to the boundary) will also show no contrast regardless of the values of $\Delta\alpha$ and $\Delta\beta$. As can be seen from Table I, the domain boundary image overlap will be due primarily to the contribution from axial astigmatism for near focus displaced aperture dark field. The image shift can be further increased by defocusing only if $\Delta\beta \neq 0$ (see Fig. 2).

The contrast of the boundary can reverse on going from over focus to underfocus of the ob-

TABLE I Image shift parameters for polyethylene single crystals at 100 keV

Boundary contrast	Diffraction conditions	$\Delta\alpha$ (rad)	$\Delta\beta$ (rad)	γ
(1 1 0) twin				
Yes	(2 0 0) and (1 1 0)	1.9×10^{-1}	1×10^{-3}	130°
Yes	(1 1 0) and (2 0 0)	1.9×10^{-1}	1×10^{-3}	130°
No	(1 $\bar{1}$ 0) and ($\bar{1}$ $\bar{1}$ 0)	9.3×10^{-4} (twin) 2.7×10^{-3} (fold)	0 (both are fold planes)	0°
(3 1 0) twin				
Yes	(1 $\bar{1}$ 0) and ($\bar{2}$ 0 0)	5.7×10^{-2}	1×10^{-3}	~ 25°
Yes	(2 0 0) and ($\bar{1}$ $\bar{1}$ 0)	5.7×10^{-2}	1×10^{-3}	
Yes	(1 1 0) and (1 $\bar{1}$ 0)	1.2×10^{-1}	0	~ 90°
{1 1 0}: {1 1 0} fold domain boundary				
Yes – 2	(2 0 0)	1.0×10^{-2}	0	90° to (0 1 0) *Ms* 0° to (1 0 0) *Ms*
No – 2				
Yes – 4	(1 1 0)	2.7×10^{-3}	1.5×10^{-5}	56° to (0 1 0) *Ms* 34° to (1 0 0) *Ms*
No – 4	(0 2 0)	0	0	–
{1 0 0}: {1 1 0} fold domain boundary				
Yes – 4	(2 0 0)	5×10^{-3}	0	varies with growth conditions
Yes – 4	(1 1 0)	1.3×10^{-3}	7.5×10^{-6}	

*Limited by radiation damage [9].

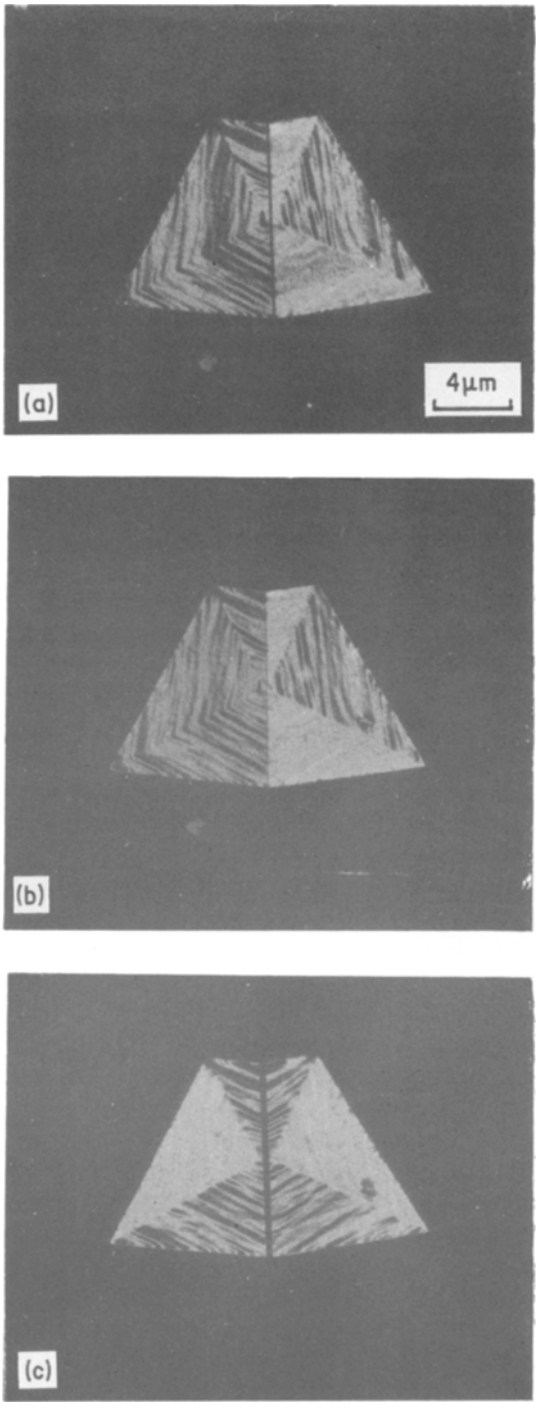

Figure 2 (3 1 0) twin boundary in polyethylene single crystal (a) and (b) illustrating the effect of defocusing the objective lens on the image overlap. In (a) the objective lens is more defocused, resulting in increased boundary width. $\mathbf{g_A} = 2\,0\,0$, $\mathbf{g_B} = 1\,1\,0$ (case illumination. (c) The same crystal imaged with $\mathbf{g_A} = 1\,1\,0$ and $\mathbf{g_B} = 1\,\bar{1}\,0$ (case i illumination). Note the increased width of the boundary between the two portions of the twin (photos courtesy of J. C. Wittmann).

jective lens since Δf reverses sign. The contrast should also reverse on going from $\mathbf{g}_1$, $\mathbf{g}_2$ to $-\mathbf{g}_1$, $-\mathbf{g}_2$ since this changes the sense of $\Delta\mathbf{g}$ by 180°. Finally, the positive overlap intensity is expected to be approximately twice the background intensity due to the overlap of two coherent images with an (unresolved) fringe pattern of spacing $1/|\Delta\mathbf{g}|$.

3. Application to various fold domain boundaries in polyethylene single crystals

3.1. (1 1 0) Twin boundary

Fig. 3 is a schematic illustration of a (1 1 0) twin boundary and the associated diffraction pattern. As can be seen from the diffraction pattern, there are three possible two beam dark-field conditions. The twin boundary will appear as a dark or bright line for $\mathbf{g_A} = 2\,0\,0$, $\mathbf{g_B} = 1\,1\,0$ and $\mathbf{g_A} = 1\,\bar{1}\,0$, $\mathbf{g_B} = 2\,0\,0$ but for $\mathbf{g_A} = \bar{1}\,\bar{1}\,0$, $\mathbf{g_B} = 1\,1\,0$, $\Delta\mathbf{g}$ is parallel to the boundary producing no contrast (see Fig. 6 of Wittmann and Kovacs [4]).

3.2. (3 1 0) Twin boundary

Fig. 4 is a schematic illustration of a (3 1 0) twin boundary and the associated diffraction pattern. The contrast behaviour of (3 1 0) type twin boundaries will be similar to that for (1 1 0) for $\mathbf{g_A} = 2\,0\,0$, $\mathbf{g_B} = \bar{1}\,\bar{1}\,0$ and $\mathbf{g_A} = 1\,\bar{1}\,0$, $\mathbf{g_B} = \bar{2}\,0\,0$ but the (3 1 0) twin boundary will also show bright or dark contrast for $\mathbf{g_A} = 1\,1\,0$, $\mathbf{g_B} = 1\,\bar{1}\,0$ since $\Delta\mathbf{g}$ in this case is nearly perpendicular to the boundary (see Fig. 4 of Wittmann and Kovacs [4]). It is also straightforward to evaluate the width of the boundary under different imaging conditions. The calculated boundary width ratio ($\Delta X'_{1\,1\,0\text{-}1\,\bar{1}\,0}/\Delta X'_{2\,0\,0\text{-}\bar{1}\,\bar{1}\,0}$) of 5 (assuming $\Delta f\Delta\beta/\Delta f_{\text{ast}} < 10^{-4}$) agrees closely with the measured value of 7 (cf. Fig. 2c and b).

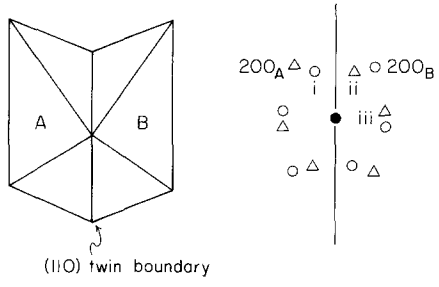

Figure 3 Schematic illustration of a (1 1 0) twin boundary in a polyethylene single crystal. Three possible two beam dark-field conditions are indicated as i–iii in the accompanying diffraction pattern.

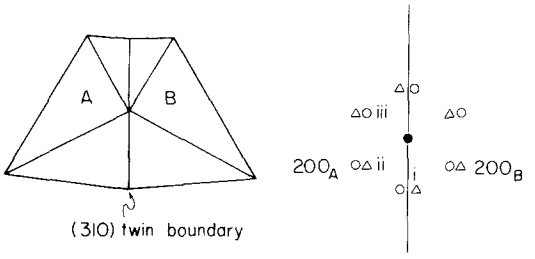

Figure 4 Schematic illustration of a (3 1 0) twin boundary in a polyethylene simple crystal. Three possible two beam dark-field conditions are indicated as i–iii in the accompanying diffraction pattern.

3.3. {1 1 0}:{1 1 0} fold domain boundaries

3.3.1. Macrosector boundaries

Since the molecules fold along {1 1 0} planes in polyethylene, any distortions due to folds will make the {1 1 0} fold planes, $(1\,1\,0)_f$, different from $\{\bar{1}\,1\,0\}$non-fold planes, $(\bar{1}\,1\,0)_{nf}$, (see Fig. 3). The distortion due to chain folding is observed in a slight splitting of the reflections [10, 11]. Bassett [6] calculated this distortion by analysis of moiré patterns from double layer crystals. Hence, depending on the imaging conditions, macrosector boundaries will show dark or bright contrast exactly analogous to twin boundaries.

For $\mathbf{g} = 1\,1\,0$ the $(1\,1\,0)_f$ planes are imaged in sectors A and C while the $(1\,1\,0)_{nf}$ planes are imaged in sectors B and D. Assuming the $(1\,1\,0)_{nf}$ plane image as fixed, we see that the $(1\,1\,0)_f$ plane image shifts so as to give boundaries $\overline{OS}$ and $\overline{OP}$ opposite contrast to $\overline{OR}$ and $\overline{OQ}$. Hence, the boundaries appear bright or dark in pairs ($\overline{OS}$, $\overline{OP}$) and $\overline{OR}$, $\overline{OQ}$).

For $\mathbf{g} = 2\,0\,0$, $\Delta\mathbf{g}$ is parallel to $\overline{OS}$ and $\overline{OQ}$ hence in 2 0 0 dark field the (1 0 0) macrosector lines show no contrast while the two (0 1 0) macrosector lines will have opposite contrast.

The contrast behaviour of macrosectors and microsectors has been previously interpreted as due to the local interaction across the fold boundary due to the asymmetrical fold protrusions which give rise to rotations of the chains in the plane of the boundary [7]. An experiment which suggests a possible test between the respective interpretations is 0 2 0 dark field in which all macrosectors vanish for the image shift interpretation (the 0 2 0 reflection is not split), whereas Bassett's model predicts that only the (0 1 0) macrosectors should vanish. However, because the diffracted intensity of the 0 2 0 reflection is only 30% of the 1 1 0 reflection, attempts to visualize macrosectors in 0 2 0 dark field have been unsuccessful. Other additional boundary features, notably the increased intensity of the macrosector boundary relative to all other areas of the dark-field image [11], and the predictability of the width of this contrast feature strongly suggest the image overlap interpretation. One would also not expect local fold interactions across the boundary to yield such sharp and strong contrast.

3.3.2. Microsector boundaries

Since microsector boundaries arise from dendritic growth where the plane chain folding changes over a short distance at the growth face, microsector boundaries are just alternating closely spaced

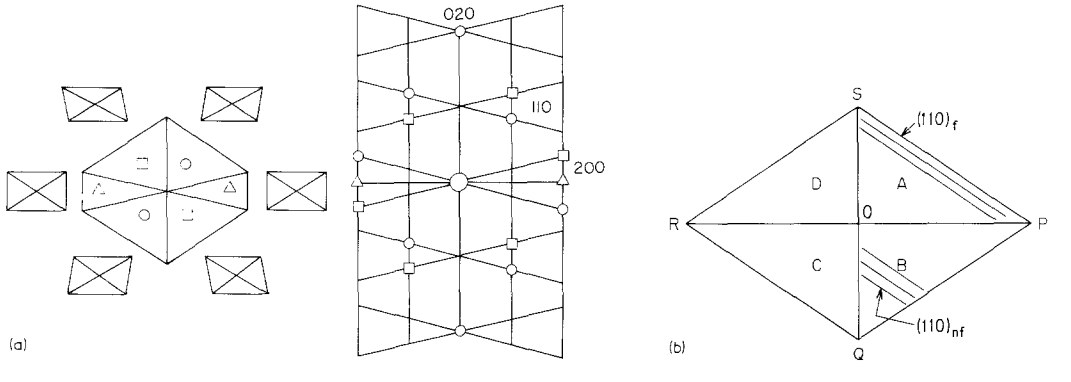

Figure 5 (a) Schematic illustration of the subcell distortion in a truncated polyethylene single crystal. The composite diffraction pattern shows the splitting of the {1 1 0} and {2 0 0} reflections (From [13]). (b) Schematic illustration of a diamond-shaped polyethylene single crystal showing the four {1 1 0} fold sections and the (1 1 0):(1 1 0) fold domain boundaries.

macrosector boundaries and thus their contrast behaviour will be identical to macrosector boundaries (see Fig. 5 of Thomas *et al.* [12]).

3.4. {1 0 0}: {1 1 0} fold domain boundaries

For crystals consisting of both {1 0 0} and {1 1 0} fold domains (truncated diamonds), there will be phase domain boundaries [1] where both the plane and direction of chain folding change. Visibility of these boundaries will, however, be limited due to the small values of $\Delta X_i'$ (see Table I).

Acknowledgement

The author wishes to thank Dr J. C. Wittmann for valuable discussions and for permission to publish Figs. 2a to c. Financial support was received from the National Science Foundation.

References

1. R. D. BURBANK, *Bell Sys. Tech. J.* **39** (1960) 1627.
2. A. AGAR, F. C. FRANK and A. KELLER, *Phil. Mag.* **4** (1959) 32.
3. I. HEBER, *Kolloid Z. u.Z. Polymere* **193** (1963) 32.
4. J. C. WITTMANN and A. J. KOVACS, *Ber. Bun. – Ges. Phys. Chem.* **74** (1970) 901.
5. D. J. BLUNDELL and A. KELLER, *J. Macro Sci.* **B2** (1968) 301.
6. D. C. BASSETT, *Phil. Mag.* **10** (1964) 595.
7. *Idem, ibid* **12** (1965) 907.
8. R. D. HEIDENREICH, W. M. HESS and L. L. BAN, *J. Appl. Crystallogr.* **1** (1968) 1.
9. E. L. THOMAS and D. G. AST, *Polymer* **15** (1974) 37.
10. S. MITSUHASI, private communication to A. Keller (1959).
11. E. L. THOMAS, S. L. SASS, and E. J. KRAMER, *J. Polymer Sci.* A2 **12** (1974) 1015.
12. E. L. THOMAS, S. L. SASS and E. J. KRAMER, *Phil. Mag.* **30** (1974) 335.
13. A. KELLER, *Rep. Prog. Phys.* **31** (1972) 623.

Received 5 May and accepted 10 June 1976.